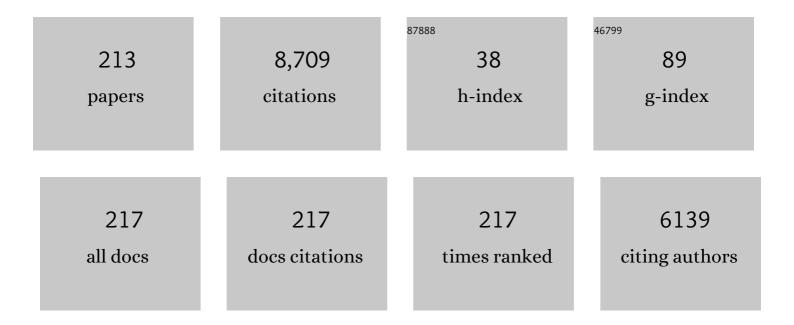
List of Publications by Year in descending order

Source: https://exaly.com/author-pdf/2838633/publications.pdf Version: 2024-02-01



IDENIA HAINSEK

#	Article	IF	CITATIONS
1	A tutorial on synthetic aperture radar. IEEE Geoscience and Remote Sensing Magazine, 2013, 1, 6-43.	9.6	1,580
2	TanDEM-X: A Satellite Formation for High-Resolution SAR Interferometry. IEEE Transactions on Geoscience and Remote Sensing, 2007, 45, 3317-3341.	6.3	1,244
3	Inversion of surface parameters from polarimetric SAR. IEEE Transactions on Geoscience and Remote Sensing, 2003, 41, 727-744.	6.3	418
4	A Network of Terrestrial Environmental Observatories in Germany. Vadose Zone Journal, 2011, 10, 955-973.	2.2	401
5	Potential of Estimating Soil Moisture Under Vegetation Cover by Means of PolSAR. IEEE Transactions on Geoscience and Remote Sensing, 2009, 47, 442-454.	6.3	253
6	TanDEM-X Pol-InSAR Performance for Forest Height Estimation. IEEE Transactions on Geoscience and Remote Sensing, 2014, 52, 6404-6422.	6.3	224
7	Tandem-L: A Highly Innovative Bistatic SAR Mission for Global Observation of Dynamic Processes on the Earth's Surface. IEEE Geoscience and Remote Sensing Magazine, 2015, 3, 8-23.	9.6	224
8	Tropical-Forest-Parameter Estimation by Means of Pol-InSAR: The INDREX-II Campaign. IEEE Transactions on Geoscience and Remote Sensing, 2009, 47, 481-493.	6.3	222
9	Very-High-Resolution Airborne Synthetic Aperture Radar Imaging: Signal Processing and Applications. Proceedings of the IEEE, 2013, 101, 759-783.	21.3	222
10	TanDEM-X: The New Global DEM Takes Shape. IEEE Geoscience and Remote Sensing Magazine, 2014, 2, 8-23.	9.6	171
11	TanDEM-X: A radar interferometer with two formation-flying satellites. Acta Astronautica, 2013, 89, 83-98.	3.2	167
12	Interferometric Synthetic Aperture Radar (SAR) Missions Employing Formation Flying. Proceedings of the IEEE, 2010, 98, 816-843.	21.3	160
13	Forest Height Estimation by Means of Pol-InSAR Data Inversion: The Role of the Vertical Wavenumber. IEEE Transactions on Geoscience and Remote Sensing, 2015, 53, 5294-5311.	6.3	148
14	Soil Moisture Estimation Under Low Vegetation Cover Using a Multi-Angular Polarimetric Decomposition. IEEE Transactions on Geoscience and Remote Sensing, 2013, 51, 2201-2215.	6.3	111
15	First Results of Rice Monitoring Practices in Spain by Means of Time Series of TerraSAR-X Dual-Pol Images. IEEE Journal of Selected Topics in Applied Earth Observations and Remote Sensing, 2011, 4, 412-422.	4.9	107
16	Polarimetric and interferometric characterization of coherent scatterers in urban areas. IEEE Transactions on Geoscience and Remote Sensing, 2006, 44, 971-984.	6.3	101
17	TanDEM-X: a terraSAR-X add-on satellite for single-pass SAR interferometry. , 0, , .		100
18	Surge dynamics and lake outbursts of Kyagar Glacier, Karakoram. Cryosphere, 2017, 11, 723-739.	3.9	89

#	Article	IF	CITATIONS
19	Quantification of Temporal Decorrelation Effects at L-Band for Polarimetric SAR Interferometry Applications. IEEE Journal of Selected Topics in Applied Earth Observations and Remote Sensing, 2013, 6, 1351-1367.	4.9	87
20	Snow Water Equivalent of Dry Snow Measured by Differential Interferometry. IEEE Journal of Selected Topics in Applied Earth Observations and Remote Sensing, 2015, 8, 3773-3790.	4.9	86
21	Ship Detection with Spectral Analysis of Synthetic Aperture Radar: A Comparison of New and Well-Known Algorithms. Remote Sensing, 2015, 7, 5416-5439.	4.0	85
22	Retrieval of agricultural crop height from space: A comparison of SARÂtechniques. Remote Sensing of Environment, 2016, 187, 130-144.	11.0	80
23	Height Estimation of Boreal Forest: Interferometric Model-Based Inversion at L- and X-Band Versus HUTSCAT Profiling Scatterometer. IEEE Geoscience and Remote Sensing Letters, 2007, 4, 466-470.	3.1	79
24	An Iterative Generalized Hybrid Decomposition for Soil Moisture Retrieval Under Vegetation Cover Using Fully Polarimetric SAR. IEEE Journal of Selected Topics in Applied Earth Observations and Remote Sensing, 2015, 8, 3911-3922.	4.9	79
25	Snow Height Determination by Polarimetric Phase Differences in X-Band SAR Data. IEEE Journal of Selected Topics in Applied Earth Observations and Remote Sensing, 2014, 7, 3794-3810.	4.9	78
26	Assessment of soil moisture effects on L-band radar interferometry. Remote Sensing of Environment, 2015, 164, 77-89.	11.0	74
27	Soil Moisture Estimation Using Hybrid Polarimetric SAR Data of RISAT-1. IEEE Transactions on Geoscience and Remote Sensing, 2016, 54, 2033-2049.	6.3	62
28	Investigation of SMAP Fusion Algorithms With Airborne Active and Passive L-Band Microwave Remote Sensing. IEEE Transactions on Geoscience and Remote Sensing, 2016, 54, 3878-3889.	6.3	58
29	First Demonstration of Agriculture Height Retrieval With PolInSAR Airborne Data. IEEE Geoscience and Remote Sensing Letters, 2012, 9, 242-246.	3.1	55
30	Validating a Notch Filter for Detection of Targets at Sea With ALOS-PALSAR Data: Tokyo Bay. IEEE Journal of Selected Topics in Applied Earth Observations and Remote Sensing, 2014, 7, 4907-4918.	4.9	55
31	Statistical Tests for a Ship Detector Based on the Polarimetric Notch Filter. IEEE Transactions on Geoscience and Remote Sensing, 2015, 53, 4578-4595.	6.3	54
32	Rice Growth Monitoring by Means of X-Band Co-polar SAR: Feature Clustering and BBCH Scale. IEEE Geoscience and Remote Sensing Letters, 2015, 12, 1218-1222.	3.1	54
33	A Statistical Test of Phase Closure to Detect Influences on <roman>DInSAR</roman> Deformation Estimates Besides Displacements and Decorrelation Noise: Two Case Studies in High-Latitude Regions. IEEE Transactions on Geoscience and Remote Sensing, 2016, 54, 5588-5601.	6.3	52
34	Soil Moisture Estimation Using Differential Radar Interferometry: Toward Separating Soil Moisture and Displacements. IEEE Transactions on Geoscience and Remote Sensing, 2017, 55, 5069-5083.	6.3	49
35	The SCALEX Campaign: Scale-Crossing Land Surface and Boundary Layer Processes in the TERENO-preAlpine Observatory. Bulletin of the American Meteorological Society, 2017, 98, 1217-1234.	3.3	49
36	EAGLE 2006 – Multi-purpose, multi-angle and multi-sensor in-situ and airborne campaigns over grassland and forest. Hydrology and Earth System Sciences, 2009, 13, 833-845.	4.9	48

#	Article	IF	CITATIONS
37	Anisotropy of seasonal snow measured by polarimetric phase differences in radar time series. Cryosphere, 2016, 10, 1771-1797.	3.9	43
38	Observations of Cutting Practices in Agricultural Grasslands Using Polarimetric SAR. IEEE Journal of Selected Topics in Applied Earth Observations and Remote Sensing, 2016, 9, 1382-1396.	4.9	43
39	Biomass estimation from polarimetric SAR interferometry over heterogeneous forest terrain. , 0, , .		42
40	Polarimetric Decomposition Over Glacier Ice Using Long-Wavelength Airborne PolSAR. IEEE Transactions on Geoscience and Remote Sensing, 2011, 49, 519-535.	6.3	39
41	A Change Detector Based on an Optimization With Polarimetric SAR Imagery. IEEE Transactions on Geoscience and Remote Sensing, 2014, 52, 4781-4798.	6.3	39
42	Large-Scale Biomass Classification in Boreal Forests With TanDEM-X Data. IEEE Transactions on Geoscience and Remote Sensing, 2016, 54, 5935-5951.	6.3	39
43	Determining Rice Growth Stage with X-Band SAR: A Metamodel Based Inversion. Remote Sensing, 2017, 9, 460.	4.0	37
44	Identification of Soil Freezing and Thawing States Using SAR Polarimetry at C-Band. Remote Sensing, 2014, 6, 2008-2023.	4.0	36
45	TanDEM-X: 10 Years of Formation Flying Bistatic SAR Interferometry. IEEE Journal of Selected Topics in Applied Earth Observations and Remote Sensing, 2021, 14, 3546-3565.	4.9	36
46	PolInSAR analysis of X-band data over vegetated and urban areas. IEEE Transactions on Geoscience and Remote Sensing, 2006, 44, 356-364.	6.3	35
47	Sub-seasonal thaw slump mass wasting is not consistently energy limited at the landscape scale. Cryosphere, 2018, 12, 549-564.	3.9	35
48	L- and P-Band 3-D SAR Reflectivity Profiles Versus Lidar Waveforms: The AfriSAR Case. IEEE Journal of Selected Topics in Applied Earth Observations and Remote Sensing, 2018, 11, 3386-3401.	4.9	34
49	Evaluation of Simplified Polarimetric Decomposition for Soil Moisture Retrieval over Vegetated Agricultural Fields. Remote Sensing, 2016, 8, 142.	4.0	33
50	Potentials and constraints of different types of soil moisture observations for flood simulations in headwater catchments. Natural Hazards, 2012, 60, 879-914.	3.4	32
51	Towards a detection of grassland cutting practices with dual polarimetric TerraSAR-X data. International Journal of Remote Sensing, 2013, 34, 8081-8103.	2.9	32
52	Single-Look SAR Tomography as an Add-On to PSI for Improved Deformation Analysis in Urban Areas. IEEE Transactions on Geoscience and Remote Sensing, 2016, 54, 6119-6137.	6.3	32
53	Applying a common allometric equation to convert forest height from Pol-InSAR data to forest biomass. , 0, , .		28
54	Classification of fully polarimetric single- and dual-frequency SAR data of sea ice using the Wishart statistics. Canadian Journal of Remote Sensing, 2005, 31, 61-72.	2.4	28

#	Article	IF	CITATIONS
55	Estimation of Rice Crop Height From X- and C-Band PolSAR by Metamodel-Based Optimization. IEEE Journal of Selected Topics in Applied Earth Observations and Remote Sensing, 2017, 10, 194-204.	4.9	28
56	A New Detection Algorithm for Coherent Scatterers in SAR Data. IEEE Transactions on Geoscience and Remote Sensing, 2015, 53, 6293-6307.	6.3	27
57	High-Resolution SAR Interferometry: Estimation of Local Frequencies in the Context of Alpine Glaciers. IEEE Transactions on Geoscience and Remote Sensing, 2008, 46, 1079-1090.	6.3	26
58	A Polarimetric First-Order Model of Soil Moisture Effects on the DInSAR Coherence. Remote Sensing, 2015, 7, 7571-7596.	4.0	26
59	Estimation of Glacier Ice Extinction Using Long-Wavelength Airborne Pol-InSAR. IEEE Transactions on Geoscience and Remote Sensing, 2013, 51, 3715-3732.	6.3	25
60	On the potential of Polarimetric SAR Interferometry to characterize theÂbiomass, moisture and structure of agricultural crops at L-,ÂC-ÂandÂX-Bands. Remote Sensing of Environment, 2018, 204, 596-616.	11.0	24
61	Polarimetric Decomposition of L-Band PolSAR Backscattering Over the Austfonna Ice Cap. IEEE Transactions on Geoscience and Remote Sensing, 2016, 54, 1267-1281.	6.3	23
62	Influence of Vegetation Growth on the Polarimetric Zero-Baseline DInSAR Phase Diversity—Implications for Deformation Studies. IEEE Transactions on Geoscience and Remote Sensing, 2016, 54, 3070-3082.	6.3	21
63	Detecting Microplastics Pollution in World Oceans Using Sar Remote Sensing. , 2018, , .		21
64	Forest Above-Ground Biomass Estimation From Vertical Reflectivity Profiles at L-Band. IEEE Geoscience and Remote Sensing Letters, 2015, 12, 2379-2383.	3.1	19
65	A Multibaseline Pol-InSAR Inversion Scheme for Crop Parameter Estimation at Different Frequencies. IEEE Transactions on Geoscience and Remote Sensing, 2016, 54, 4952-4970.	6.3	19
66	Mapping Retrogressive Thaw Slumps Using Single-Pass TanDEM-X Observations. IEEE Journal of Selected Topics in Applied Earth Observations and Remote Sensing, 2020, 13, 3263-3280.	4.9	19
67	Removal of additive noise in polarimetric eigenvalue processing. , 0, , .		18
68	TanDEM-X: mission concept and performance analysis. , 0, , .		18
69	Polarimetric SAR Time Series Change Analysis Over Agricultural Areas. IEEE Transactions on Geoscience and Remote Sensing, 2020, 58, 7317-7330.	6.3	18
70	Pol-InSAR for agricultural vegetation parameter estimation. , 0, , .		16
71	Polarimetric Calibration of the Ku-Band Advanced Polarimetric Radar Interferometer. IEEE Transactions on Geoscience and Remote Sensing, 2018, 56, 2295-2311.	6.3	16
	Call Matteries Fatheration in the antitle D In CAD - 2009		

#	Article	IF	CITATIONS
73	MAPSAR: a small L-band SAR mission for land observation. Acta Astronautica, 2005, 56, 35-43.	3.2	14
74	3-D Scattering Characterization of Agricultural Crops at C-Band Using SAR Tomography. IEEE Transactions on Geoscience and Remote Sensing, 2018, 56, 3976-3989.	6.3	14
75	ALOS-Next/TanDEM-L: A highly innovative SAR mission for global observation of dynamic processes on the earth's surface. , 2015, , .		13
76	Ship Detection With TanDEM-X Data Extending the Polarimetric Notch Filter. IEEE Geoscience and Remote Sensing Letters, 2015, 12, 2160-2164.	3.1	13
77	Multipath Interferences in Ground-Based Radar Data: A Case Study. Remote Sensing, 2017, 9, 1260.	4.0	13
78	Assessment of Paddy Rice Height: Sequential Inversion of Coherent and Incoherent Models. IEEE Journal of Selected Topics in Applied Earth Observations and Remote Sensing, 2018, 11, 3001-3013.	4.9	13
79	Modeling and Compensation of the Penetration Bias in InSAR DEMs of Ice Sheets at Different Frequencies. IEEE Journal of Selected Topics in Applied Earth Observations and Remote Sensing, 2020, 13, 2698-2707.	4.9	12
80	Cross-Correlation Stacking for Robust Offset Tracking Using SAR Image Time-Series. IEEE Journal of Selected Topics in Applied Earth Observations and Remote Sensing, 2021, 14, 4765-4778.	4.9	12
81	Assessing volumetric change distributions and scaling relations of retrogressive thaw slumps across the Arctic. Cryosphere, 2022, 16, 1-15.	3.9	12
82	Comparing Performances of Crop Height Inversion Schemes From Multifrequency Pol-InSAR Data. IEEE Journal of Selected Topics in Applied Earth Observations and Remote Sensing, 2017, 10, 1727-1741.	4.9	11
83	Impact of Plant Surface Moisture on Differential Interferometric Observables: A Controlled Electromagnetic Experiment. IEEE Transactions on Geoscience and Remote Sensing, 2017, 55, 3949-3964.	6.3	11
84	Sensitivity of SAR Tomography to the Phenological Cycle of Agricultural Crops at X-, C-, and L-band. IEEE Journal of Selected Topics in Applied Earth Observations and Remote Sensing, 2018, 11, 3014-3029.	4.9	11
85	Modeling the Vertical Backscattering Distribution in the Percolation Zone of the Greenland Ice Sheet With SAR Tomography. IEEE Journal of Selected Topics in Applied Earth Observations and Remote Sensing, 2019, 12, 4389-4405.	4.9	11
86	A Case Study on the Correction of Atmospheric Phases for SAR Tomography in Mountainous Regions. IEEE Transactions on Geoscience and Remote Sensing, 2019, 57, 416-431.	6.3	11
87	Geostatistical Analysis and Mitigation of the Atmospheric Phase Screens in Ku-Band Terrestrial Radar Interferometric Observations of an Alpine Glacier. IEEE Transactions on Geoscience and Remote Sensing, 2020, 58, 7533-7556.	6.3	11
88	3-D structure observation of African tropical forests with multi-baseline SAR: Results from the AfriSAR campaign. , 2017, , .		10
89	A Multi-Year Study on Rice Morphological Parameter Estimation with X-Band Polsar Data. Applied Sciences (Switzerland), 2017, 7, 602.	2.5	10
90	Modeling Multifrequency Pol-InSAR Data From the Percolation Zone of the Greenland Ice Sheet. IEEE Transactions on Geoscience and Remote Sensing, 2019, 57, 1963-1976.	6.3	10

#	Article	IF	CITATIONS
91	Polarimetric Behavior for the Derivation of Sea Ice Topographic Height From TanDEM-X Interferometric SAR Data. IEEE Journal of Selected Topics in Applied Earth Observations and Remote Sensing, 2021, 14, 1095-1110.	4.9	10
92	Depth-Resolved Backscatter and Differential Interferometric Radar Imaging of Soil Moisture Profiles: Observations and Models of Subsurface Volume Scattering. IEEE Journal of Selected Topics in Applied Earth Observations and Remote Sensing, 2017, 10, 3281-3296.	4.9	9
93	On the Separation of Ground and Volume Scattering Using Multibaseline SAR Data. IEEE Geoscience and Remote Sensing Letters, 2017, 14, 1570-1574.	3.1	9
94	MOSES: A Novel Observation System to Monitor Dynamic Events across Earth Compartments. Bulletin of the American Meteorological Society, 2022, 103, E339-E348.	3.3	9
95	Soil moisture retrieval under agricultural vegetation using fully polarimetric SAR. , 2012, , .		8
96	Polarimetric 3-D imaging with airborne holographic SAR tomography over glaciers. , 2015, , .		8
97	The global TanDEM-X DEM — A unique data set. , 2017, , .		8
98	Model-Based Interpretation of PolSAR Data for the Characterization of Glacier Zones in Greenland. IEEE Journal of Selected Topics in Applied Earth Observations and Remote Sensing, 2021, 14, 11593-11607.	4.9	8
99	Spaceborne SAR tomography in urban areas. , 2013, , .		7
100	Ship detectors exploiting spectral analysis of SAR images. , 2014, , .		7
101	Interferometric and polarimetric methods to determine SWE, fresh snow depth and the anisotropy of dry snow. , 2015, , .		7
102	Tandem-L: Project Status and Main Findings of the Phase Bl Study. , 2018, , .		7
103	Accelerated mobilization of organic carbon from retrogressive thaw slumps on the northern Taymyr Peninsula. Cryosphere, 2022, 16, 2819-2835.	3.9	7
104	SAR tomography based 3-D point cloud extraction of point-like scatterers in urban areas. , 2014, , .		6
105	Statistical Tests for Symmetries in Polarimetric Scattering Coherency Matrices. IEEE Geoscience and Remote Sensing Letters, 2014, 11, 308-312.	3.1	6
106	TanDEM-X: Science activities. , 2015, , .		6
107	Global sensitivity analysis of a morphology based electromagnetic scattering model. , 2015, , .		6
108	Dual-polarimetric agricultural change analysis of long baseline TanDEM-X time series data. , 2016, , .		6

#	Article	IF	CITATIONS
109	Tandem-L: Main results of the phase a feasibility study. , 2016, , .		6
110	Wet Snow Depth from Tandem-X Single-Pass Insar Dem Differencing. , 2018, , .		6
111	A Motion Compensation Strategy for Airborne Repeat-Pass SAR Data. IEEE Geoscience and Remote Sensing Letters, 2018, 15, 1580-1584.	3.1	6
112	Separating the Influence of Vegetation Changes in Polarimetric Differential SAR Interferometry. IEEE Transactions on Geoscience and Remote Sensing, 2018, 56, 6871-6883.	6.3	6
113	Joint PAZ & TanDEM-X Mission Interferometric Experiments: Interoperability and Products. IEEE Journal of Selected Topics in Applied Earth Observations and Remote Sensing, 2021, 14, 6069-6082.	4.9	6
114	Calibration and Operation of a Bistatic Real-Aperture Polarimetric-Interferometric Ku-Band Radar. IEEE Transactions on Geoscience and Remote Sensing, 2022, 60, 1-19.	6.3	6
115	Comparison of ship detectors using polarimetric alos data: Tokyo Bay. , 2013, , .		5
116	On the Interpretation of Polarimetric Phase Differences in SAR Data Over Land Ice. IEEE Geoscience and Remote Sensing Letters, 2016, 13, 192-196.	3.1	5
117	Polarimetric Analysis of Natural Terrain Observed With a <i>Ku</i> Band Terrestrial Radar. IEEE Journal of Selected Topics in Applied Earth Observations and Remote Sensing, 2019, 12, 5268-5288.	4.9	5
118	Efficient Approach for Atmospheric Phase Screen Mitigation in Time Series of Terrestrial Radar Interferometry Data Applied to Measure Glacier Velocity. IEEE Journal of Selected Topics in Applied Earth Observations and Remote Sensing, 2021, 14, 7734-7750.	4.9	5
119	Self-Supervised Pretraining and Controlled Augmentation Improve Rare Wildlife Recognition in UAV Images. , 2021, , .		5
120	Forest characterisation by means of TerraSAR-X and TanDEM-X (polarimetric and) interferometric data. , 2011, , .		4
121	Active and passive L-band microwave remote sensing for soil moisture — A test-bed for SMAP fusion algorithms. , 2014, , .		4
122	Vertical forest structure characterization for the estimation of above ground biomass: First experimental results using SAR vertical reflectivity profiles. , 2014, , .		4
123	SAR tomography for spatio-temporal inversion of point-like scatterers in urban areas. , 2015, , .		4
124	PolSAR-Ap: Exploitation of fully polarimetric SAR data for application demonstration. , 2015, , .		4
125	TanDEM-X mission status: The complete new topography of the Earth. , 2016, , .		4
126	SAR imaging of tropical African forests with P-band multibaseline acquisitions: Results from the		4

AfriSAR campaign. , 2016, , .

#	Article	IF	CITATIONS
127	Sensitivity of polarimetric SAR interferometry data to different vertical subsurface structures of the Greenland ice sheet. , 2017, , .		4
128	Analyzing the Influence of Wet Biomass Changes in Polarimetric Differential SAR Interferometry at <i>L</i> Band. IEEE Journal of Selected Topics in Applied Earth Observations and Remote Sensing, 2018, 11, 1494-1508.	4.9	4
129	Verification of the Virtual Bandwidth SAR Scheme for Centimetric Resolution Subsurface Imaging From Space. IEEE Transactions on Geoscience and Remote Sensing, 2018, 56, 25-34.	6.3	4
130	An Experimental Car-Borne SAR System: Measurement Setup and Positioning Error Analysis. , 2018, , .		4
131	A Car-Borne SAR System for Interferometric Measurements: Development Status and System Enhancements. , 2018, , .		4
132	Tandem-X: Mission Status and Science Activities. , 2019, , .		4
133	Sensitivity Analysis of Bistatic Scattering for Soil Moisture Retrieval. Remote Sensing, 2021, 13, 188.	4.0	4
134	Towards the Integration of SAR Tomography and PSI for Improved Deformation Assessment in Urban Areas. , 2015, , .		4
135	Refined soil moisture estimation by means of L-band polarimetry. , 2013, , .		3
136	Observational analysis of soil moisture effects on DInSAR signals. , 2013, , .		3
137	Phenological growth stages of paddy rice according to the BBCH scale and SAR images. , 2014, , .		3
138	Agricultural monitoring with polarimetric SAR time series. , 2015, , .		3
139	Investigating the combined use of differential SAR tomography and PSI for spatio-temporal inversion. , 2015, , .		3
140	SAR Tomography as an Add-On to PSI: Detection of Coherent Scatterers in the Presence of Phase Instabilities. Remote Sensing, 2018, 10, 1014.	4.0	3
141	Glacier Detachment Hazard Analysis in the West Kunlun Shan Mountains. , 2019, , .		3
142	KAPRI: A Bistatic Full-Polarimetric Interferometric Real-Aperture Radar System for Monitoring of Natural Environments. , 2021, , .		3
143	Retrieval of Firn Thickness by Means of Polarisation Phase Differences in L-Band SAR Data. Remote Sensing, 2021, 13, 4448.	4.0	3
144	Antarctic snow-covered sea ice topography derivation from TanDEM-X using polarimetric SAR interferometry. Cryosphere, 2021, 15, 5323-5344.	3.9	3

#	Article	IF	CITATIONS
145	Comparison of helicopter-borne thin sea ice thickness profiles with polarimetric signatures of dual-pol Terrasar-X data. , 2009, , .		2
146	Linking the polarimetric change detector based on perturbation filters with the Pol-InSAR coherence. , 2012, , .		2
147	Polarimetric soil moisture retrieval using an iterative generalized hybrid decomposition technique. , 2014, , .		2
148	Scattering centers monitoring in refocused SAR images on a high-resolution DEM. , 2014, , .		2
149	A new algorithm for iceberg detection with dual-polarimetric SAR data. , 2015, , .		2
150	Retrieval of soil moisture using multi-temporal hybrid polarimetric RISAT-1 data. , 2015, , .		2
151	3-D glacier subsurface characterization using SAR polarimetry. , 2015, , .		2
152	On the estimation of agricultural crop height from Pol-InSAR data. , 2015, , .		2
153	Physically-based active-passive modelling and retrieval for SMAP soil moisture inversion algorithm. , 2015, , .		2
154	Monitoring permafrost and thermokarst processes with TanDEM-X DEM time series: Opportunities and limitations. , 2016, , .		2
155	SAR tomography as an add-on to PSI: Gain in deformation sampling vis-a-vis quality of the detected scatterers. , 2016, , .		2
156	Morphology estimation of rice fields using X-band PolSAR data. , 2016, , .		2
157	Multi-dimensional airborne holographic SAR tomography reconstruction for glaciers at L-/P-band. , 2016, , .		2
158	Tandem-X: Science Activities. , 2018, , .		2
159	Seven Years of Tandem-X: Volume Loss of Grosser Aletschgletscher, Switzerland. , 2018, , .		2
160	Trajectory Uncertainty in Repeat-Pass SAR Interferometry: A Case Study. , 2019, , .		2
161	TanDEM-X: Das neue globale Höhenmodell der Erde. , 2015, , 1-30.		2
162	Theory of radar polarimetric interferometry and its application to the retrieval of sea ice elevation in the Western Weddell Sea, Antarctic. Earth and Space Science, 0, , .	2.6	2

#	Article	IF	CITATIONS
163	Relating co-polarization phase difference at L-band over land ice to the structure of snow and firn layers. , 2014, , .		1
164	The impact of vegetation growth on DInSAR coherence regions and estimated deformations. , 2014, , .		1
165	Monitoring floods in the Kafue flats with TanDEM-X data. , 2015, , .		1
166	Applications of integrals of quadratic forms for polarimetric SAR data. , 2015, , .		1
167	TanDEM-X: A single-pass SAR interferometer for global DEM generation and demonstration of new SAR techniques. , 2015, , .		1
168	Spatial and temporal characterization of agricultural crop volumes by means of polarimetric SAR tomographyatc-band. , 2015, , .		1
169	Sar algorithms for crop height estimation: The paddy-rice case study. , 2016, , .		1
170	First study on holographic SAR tomography over agricultural crops at C-/X-band. , 2016, , .		1
171	A case study on the use of differential SAR tomography for measuring deformation in layover areas in rugged alpine terrain. , 2017, , .		1
172	Single-baseline polarimetric SAR interferometry for characterizing the biophysical properties of agricultural crops. , 2017, , .		1
173	Single pass InSAR missions for monitoring hazardous surging glaciers. , 2017, , .		1
174	TanDEM-X: Science activities. , 2017, , .		1
175	Geostatistical Analysis and Mitigation of Atmospheric Phase Screens in Ku-Band Terrestrial Radar Interferometry. , 2018, , .		1
176	Radar Remote Sensing of Land Surface Parameters. Ecohydrology, 2018, , 1-38.	0.2	1
177	Interpretation of Polarimetric and Tomographic Signatures from Glacier Subsurface: the K-Transect Case Study. , 2019, , .		1
178	Correction to "A Statistical Test of Phase Closure to Detect Influences on DInSAR Deformation Estimates Besides Displacements and Decorrelation Noise: Two Case Studies in High-Latitude Regions― [Sep 16 5588-5601]. IEEE Transactions on Geoscience and Remote Sensing, 2019, 57, 623-623.	6.3	1
179	Technical Committees Survey Results [Technical Committees]. IEEE Geoscience and Remote Sensing Magazine, 2020, 8, 90-95.	9.6	1
180	Cryosphere Applications. Remote Sensing and Digital Image Processing, 2021, , 179-213.	0.7	1

#	Article	IF	CITATIONS
181	Agriculture and Wetland Applications. Remote Sensing and Digital Image Processing, 2021, , 119-178.	0.7	1
182	Tandem-X: Mission and Science. , 2021, , .		1
183	TanDEM-X. , 2017, , 525-554.		1
184	TanDEM-X: 10 Years of Operation. , 2020, , .		1
185	Introduction to the Special Section on Temporal Change Observation for Bio-Geophysical Parameters. IEEE Journal of Selected Topics in Applied Earth Observations and Remote Sensing, 2011, 4, 400-401.	4.9	0
186	Orientation effects on polarimetric SAR images of sea ice. , 2013, , .		0
187	Recent advances on SAR polarimetry to observe surfactants and targets at sea. , 2013, , .		0
188	Foreword to the Special Issue on the 2012 IEEE International Geoscience and Remote Sensing Symposium (IGARSS'12). IEEE Journal of Selected Topics in Applied Earth Observations and Remote Sensing, 2013, 6, 1068-1069.	4.9	0
189	Modelling the impact of moisture changes in a heterogeneous soil on differential interferometry. , 2014, , .		0
190	Processing polarimetric SAR time series over urban areas with binary partition trees. , 2015, , .		0
191	Development of new multi-band equatorially orbiting POLinSAR satellite sensors system configurations for varying latitudinal coverage within total tropical belt: Invited group presentation for establishing an associated Consortium. , 2015, , .		0
192	IGARSS 2014 Survey Results [Conference Reports]. IEEE Geoscience and Remote Sensing Magazine, 2015, 3, 57-59.	9.6	0
193	A preliminary analysis of component polarimetric decomposition towards soil moisture inversion in an oasis of the northwest arid regions of China. , 2016, , .		0
194	Imaging subsurface soil moisture dynamics using tomopgraphic profiling: Observations and modelling. , 2016, , .		0
195	Volume structure characterisation by means of multi-baseline Pol-InSAR: Status and challenges. , 2016, , .		0
196	Virtual bandwith SAR (VB-SAR) for centimeter-scale vertical profiling through a soil at C-band from space. , 2016, , .		0
197	Time series investigation of soil moisture estimation using compact polarimetry at L-band. , 2016, , .		0

198 Using metamodels for agricultural monitoring. , 2016, , .

#	Article	IF	CITATIONS
199	Corrections to "Single-Look SAR Tomography as an Add-On to PSI for Improved Deformation Analysis in Urban Areas―[Oct 16 6119-6137]. IEEE Transactions on Geoscience and Remote Sensing, 2017, 55, 1854-1854.	6.3	0
200	Agricultural biomass maps based on polarimetric differential SAR interferometry. , 2017, , .		0
201	Future mission concepts for measuring snow mass. , 2017, , .		0
202	SAR Tomography for Spatio-Temporal Inversion of Coherent Scatterers in Villages of Alpine Regions. , 2018, , .		0
203	Assessment of the Ground Polarimetry in Crops Estimated Using MB Sar Interferometry at C-Band. , 2018, , .		0
204	Foreword to the Special Issue on Forest Structure Estimation in Remote Sensing. IEEE Journal of Selected Topics in Applied Earth Observations and Remote Sensing, 2018, 11, 3384-3385.	4.9	0
205	Determination of rice plant morphology by stochastic optimization using X-band polsar data. , 2018, , .		0
206	Radar Remote Sensing of Land Surface Parameters. Ecohydrology, 2019, , 379-416.	0.2	0
207	A Comparison of Tropospheric Path Delays Estimated in PSI Processing Against Delays Derived from a GNSS Network in the Swiss Alps. , 2019, , .		0
208	Polsar Data Compensation of Steep Terrain With Application To Soil Moisture Retrival. , 2019, , .		0
209	Investigating the Potential to Estimate Insar Penetration Depth Over Ice Sheets from Pol-Insar Data. , 2019, , .		0
210	IGARSS 2019 in Yokohama, Japan: Events and New Directions [Conference Reports]. IEEE Geoscience and Remote Sensing Magazine, 2019, 7, 37-48.	9.6	0
211	Complementarity and Potential of Polsar and Tomosar for Glacier Subsurface Characterization. , 2021,		0
212	Foreword to the Special Issue on the 2019 IEEE International Geoscience and Remote Sensing Symposium (IGARSS 2019). IEEE Journal of Selected Topics in Applied Earth Observations and Remote Sensing, 2020, 13, 6512-6514.	4.9	0
213	Polarimetric Characteristics for Sea-Ice Surface Topographic Derivation Using TanDEM-X Interferometry Data. , 2020, , .		0

13